Light Metals 2014
Edited by: John Grandfield
TMS (The Minerals, Metals & Materials Society), 2014

Revised Benchmark Problem for Modeling of Metal Flow and Metal Heaving in Reduction Cells

Jinsong Hua[1], Christian Droste[2], Kristian E. Einarsrud[3], Magne Rudshaug[1], Robert Jorgensen[4], Nils-Haavard Giskeodegard[4]

[1] Dept. of Computational Materials Processing, Institute for Energy Technology, N-2027 Kjeller, Norway
[2] Hydro Aluminium Deutschland GmbH, Primary Metal Technology, 41468 Neuss, Germany
[3] SINTEF Materials and Chemistry, N–7465 Trondheim, Norway
[4] Hydro Aluminium, N-6882 Øvre Årdal, Norway

Keywords: MHD, metal heaving, metal flow, computational fluid dynamics

Abstract

Stationary metal flow and metal heaving impact both heat balance and cell stability and affects pot tending as well. For improving cell performance and productivity, a good knowledge of these quantities is indispensable. However, limited access restricts the precise determination of the metal flow and heaving by measurements, and sought information must thus be derived from mathematical modeling of the magnetohydrodynamic (MHD) flow. The literature is scarce when it comes to benchmark problems for MHD flow in a cell and those cases which are available often suffer from insufficient level of detail, lack of input data and some inconsistencies. In this paper, a benchmark problem is given, resolving the deficiencies identified in the literature. A newly developed MHD model based on ANSYS FLUENT and User Defined Functions is applied to simulate the resulting flow pattern and interface heaving of the two immiscible bath/metal fluids in reduction cells.

Introduction

In a Hall-Héroult cell, aluminium is formed at the interface of the electrolyte (bath) and the liquid metal. The electrolyte is floating on top of the liquid metal layer (metal) due to the density difference. Electromagnetic forces lead to a steady movement of the two superimposed liquids and a deformation of the metal-bath interface. These MHD phenomena can limit both the current and energy efficiency of the process as well as hampering pot operation and process control. Strong metal heaving caused by the differences of the electromagnetic forces between metal and bath is also quite cumbersome with respect to anode change [3] and achievement of low anode gross consumption without jeopardizing the Fe content of the liquid metal by flooding the anodes. In addition, metal-bath interface instabilities coupled to the background flow and metal pad deformation can occur [1-2] which disturb the process harmfully.

Consequently, a quantitative prediction of both the melts flow and the bath-metal interface deformation [2] is critical for the design and operation of alumina reduction cells. To achieve this with up-to-date computational fluid dynamics (CFD) tools, a new multiphase flow model based on ANSYS FLUENT was developed. By applying so called User Defined Functions (UDF) the coupling between liquid flow, interface deformation, electrical potential, current density distribution and the Lorentz force was realized. Special efforts were paid not only to precisely track the metal-bath interface by using the volume of fluid (VOF) method, but also to allow for anode burn-off to ensure a constant anode-cathode distance. The latter is a necessary prerequisite for accurate modeling of metal heaving also as initial condition for the simulation of metal pad redistribution after anode change [3, 6]. A UDF was developed to calculate the vertical distance between metal interface and anode bottom at each time step for adjusting the bottom of the anodes with respect to the metal interface. In addition the sliding mesh method of ANSYS FLUENT is applied.

The calculation of the electric currents crossing the bath-metal interface as one contributor to the electromagnetic forces requires a careful treatment of the strong varying electrical conductivities at the interface which is implemented by UDFs as well.

With main focus on metal flow and metal heaving, the effects due to gas bubbles, which are important for the bath flow, are not considered here.

One main challenge in the development of such a highly complex simulation is the lack of well-known solutions for model verification. In [4], a series of benchmark problems are formulated addressing this issue. However, it turned out that the some relevant information is missing to allow for an unambiguous comparison. Therefore, some important supplementary details are given here which should make a comparison less challenging by limiting the choice of not specified parameters. Crucial parameters like mesh density which controls the resolution of forces and hence deformation, boundary conditions, discretization, a complete set of required material properties, and timescale for the transient computation are reported.

Fundamentals and governing equations

Governing equations of VOF method for fluid flow

The Volume of Fluid (VOF) method can be used to simulate the dynamics of a two immiscible fluid system by solving a single set of momentum and continuity equations, and track the distribution of volume fraction of each fluid throughout the computational domain. The VOF formulation is generally used to compute a time-dependent solution. The governing equations of the continuity and momentum conservation for a two-phase flow system with incompressible fluids are expressed as:

$$\nabla \cdot \mathbf{u} = 0 \tag{1}$$

$$\frac{\partial}{\partial t}(\rho \mathbf{u}) + \nabla \cdot (\rho \mathbf{u}\mathbf{u}) = -\nabla P + \nabla \cdot \left[\mu\left(\nabla \mathbf{u} + \nabla \mathbf{u}^T\right)\right] + \mathbf{F}_E + \rho \mathbf{g} \tag{2}$$

where **u** represents the flow field, and P is the pressure. **g** refers to the gravitational acceleration and $\mathbf{F}_E$ represents the external body force density, such as electromagnetic forces. ρ and μ are the fluid density and viscosity, respectively. For a two-fluid system, the fluid properties (ρ and μ) are calculated with fluid volume fraction weighted averaging:

$$\rho = \rho_1\alpha_1 + \rho_2\alpha_2 \quad (3)$$

$$\mu = \mu_1\alpha_1 + \mu_2\alpha_2 \quad (4)$$

where the subscripts 1 and 2 denote the primary phase and the secondary phase, respectively, and α the fluid volume fraction.

The distribution of the volume fraction for each phase and the tracking of the phase-interface are accomplished by solving the continuity equation for the volume fraction of the secondary phase (α_2)

$$\frac{\partial\alpha_2}{\partial t} + \mathbf{u}\cdot\nabla\alpha_2 = 0 \quad (5)$$

The primary-phase volume fraction (α_1) will be determined by the phase continuity constraint: $\alpha_1 = 1-\alpha_2$. In Fluent, various numerical approaches are implemented for solving the secondary phase volume fraction equation (5). In this paper, the geometric reconstruction scheme is adopted to maintain the interface sharpness while it is moving and deforming.

Equations for electrical field and Lorentz force distribution

The Lorentz force is needed to close the governing equations for fluid flow. The electric current density **J** is calculated from Ohm's law taking into account the induced currents caused by the moving conductive liquid with velocity **u** in an external magnetic field **B**:

$$\mathbf{J} = -\sigma\nabla\varphi + \sigma\,\mathbf{u}\times\mathbf{B} \quad (5)$$

Current conservation implies that the electrical potential f is solution of the potential equation

$$\nabla\cdot\sigma\nabla\varphi = \nabla(\sigma\,\mathbf{u}\times\mathbf{B}) \quad (6)$$

For simplicity, locally induced magnetic fields will be neglected in the current approach.
A volume fraction weighted harmonic average method is mandatory to correctly calculate the distribution of electrical conductivity over the metal-bath interface and conserve the electric current in the numerical discretization of (6):

$$\frac{1}{\sigma} = \frac{\alpha_1}{\sigma_1} + \frac{\alpha_2}{\sigma_2} \quad (7)$$

The Lorentz force density is given as

$$\mathbf{F}_E = \mathbf{J}\times\mathbf{B}\ , \quad (8)$$

where **B** in this current work is a *predefined* magnetic field mimicking that expected in a conventional cell. The calculated Lorentz force is included in the source term ($\mathbf{F}_E$) of the momentum equation (2).

Turbulence

To limit the complexity of the problem, the standard k-ε turbulence model with standard wall functions is solved to calculate the turbulent viscosity in the each phase. This will allow for easy repeatability, which is the main focus of such a benchmark.

The deficiencies of the k-ε turbulence model for such type of flow where recirculation and re-attachment at the boundary layer could occur are well known [5]. A $k-\omega$ turbulence model would probably be a better choice, but ultimately requires an exceedingly fine meshing of the boundary layer for the current application.

In the previous benchmark case [4], the eddy-viscosity approach to generate turbulent viscosity was chosen. However, quite different viscosity settings were needed by the various codes (Shallow Layer, ESTER/PHOENICS and ANSYS/CFX) to recalculate the published interface shape. The portability of this approach to different CDF codes seems not to be satisfactory.

Revised benchmark case

General set-up

Compared to Severo's benchmark model [4], a somewhat larger size was chosen to allow for a today's more representative cell with amperage of around 300 kA. The definition of the cathode current distribution follows closely the representation as given in [4], while the externally imposed magnetic field is chosen to be closer to the field of real cells, i. e. less symmetric.

To take into account the consumption of anodes in the reduction process, the model keeps constant ACD by moving the anode bottom according to the height of the bath-metal interface. At each time step every node of the anode bottom is adjusted in course of the interface movement alteration. In ANSYS FLUENT, the dynamic mesh and sliding meshing technique is applied to achieve this.

Geometry

A rectangular box model, which has the dimensions close to real cells, is shown in Figure 1. It has a length of 12 m and width of 4 m. The height of metal layer is 0.2 m, and the bath layer height is 0.18 m. The distance between anode and metal-bath interface (ACD) is set to be 0.045 m. The cell consists of twenty anodes. The width of central and side channels is 0.15 m, and the width of cross channels is 0.05 m.

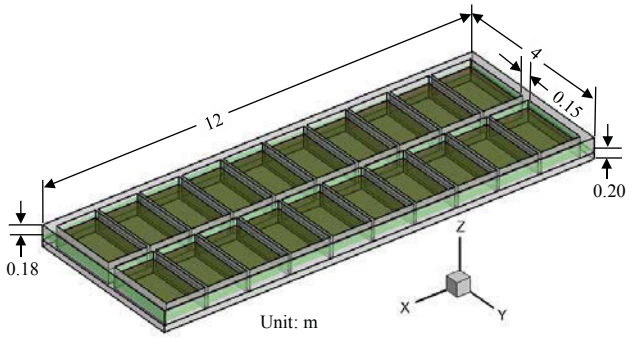

Figure 1: Geometry of the Box model for an alumina reduction cell.

The computational mesh used for the CFD analysis is shown in Figure 2. In general hexahedral cells are used. In the horizontal

directions, the central channel and cross channel are meshed with four computational cells, the side channel is meshed with six cells and each anode is meshed with 20×12 cells. In the vertical direction, the model is divided into three zones. The top zone covering the channel height (bath above ACD) is meshed with eight cells. The middle zone is the interface deformation zone. It has a thickness of 0.08 m which covers the ACD height and part of metal layer. It is meshed with ten cells to capture the interface deformation. The bottom zone, which has a height of 0.12 m, is meshed with six mesh grids. The CFD model contains 187,392 hexahedral cells.

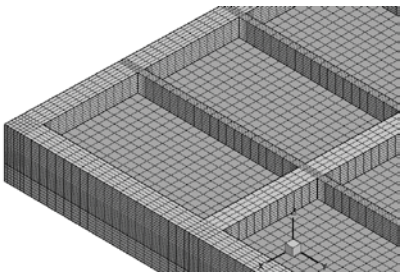

Figure 2: CFD mesh used for the numerical simulation.

To investigate the effect of cross channels on the simulation results, a second CFD model which neglects the cross channels, but keeps both central channel and side channels was created. Hence such a simplified CFD model consists of only two large anodes as shown in Figure 3.

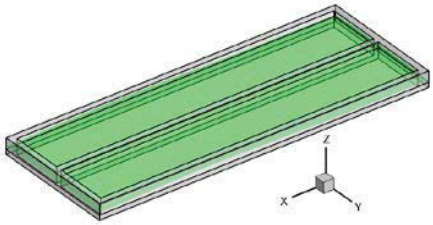

Figure 3: A simplified box model for an alumina reduction cell neglecting the cross channels.

Fluid properties

In the CFD model setup, the material properties for the fluids, electrolyte and liquid aluminum are required; they are summarized in Table 1.

Table 1: Material Properties

Property	Unit	Electrolyte	Liquid Aluminum
Density	kg/m^3	2070	2270
Viscosity	mPa s	1.25	2.5
El. conductivity	S m^{-1}	250	3.0E6

Boundary conditions

For fluid flow, no slip boundary conditions are applied on all wall surfaces. The free surface on top of the bath is ignored by applying no slip boundary conditions as well. Standard wall functions are assumed on all solid walls for solving of the k-ε turbulence model.

As boundary for the electric potential equation, zero electric potential is set on the bottom and side of anode. Of course, in a more complete model, the anodes should be included as well and the constant potential should then be applied on top of the anodes. Electrical insulation conditions are applied on the reduction cell side walls, where the current density is set zero. Since the fluid velocity on the side walls is assumed zero, the zero-flux condition is used for the electrical potential calculation. The normal current density (A/m^2) on the top of cathode surface is specified explicitly as

$$J_z = -2181 - 3013y^2 . \tag{9}$$

The external magnetic field (mT) imposed upon both bath and metal layers inside the reduction cell is assumed as,

$$\begin{cases} B_x = -1.5 - 0.2x + 8.0y - 0.05xy \\ B_y = -0.7 - 1.0x + 0.2y - 0.01xy \\ B_z = -0.02 - 0.1x - 0.5y - 0.7xy \end{cases} \tag{10}$$

Both the prescribed normal current density J_z and the imposed magnetic field **B** show the main characteristics of those of real cells, increasing current pick-up along the cathode block and the magnetic field pattern as a superposition of magnetic fields generated by the external and cell internal currents carrying parts.

As in the previous benchmark [4], the Ampere-Maxwell equation

$$\nabla \times \boldsymbol{B} = \mu_0 \boldsymbol{J} \tag{11}$$

is not fulfilled for the artificial magnetic field and the chosen current boundary condition for electrical current density. However, this will not lead to any inconsistencies in the simulations because equation (11) is not utilized in the model.

Initial conditions

The fluid velocity inside the reduction cell is assumed to be zero. The electric potential is set zero as well. The metal/bath interface is initialized as a flat horizontal surface with a height of 0.2 m. The bath layer rests above the liquid metal layer.

Simulation conditions

In general, simple numerical schemes provided by ANSYS FLUENT were applied: "SIMPLE" for pressure-velocity coupling, the spatial discretization scheme "PRESTO!" for pressure, the "Geo-Reconstruct" scheme for volume fraction, and "First Order Upwind" for other equations.

Transient simulation is adopted in the modeling. "First Order Implicit" scheme is applied for the transient formulation. The time step size is set constant as 0.04s. The steadiness of the transient simulation results is estimated by averaging the transient data over a certain period of 4s. It is found that the simulations reach quasi-steady state after 240s simulation time (6000 time steps). The results presented in this paper are the simulation data at 240s or 6000 time steps.

Results and discussion

Simulation for an analytical test case

To test the basic capability of the CFD model, it was used to predict the bath-metal interface deformation under the effect of a specified hydrostatic force. The model configuration was based on Severo's benchmark case [4]. An irrotational force field

$$F_x = -25 \cdot x \ \text{N/m}^3 \,, F_y = 0.0 \ \text{N/m}^3 \,, F_z = 0.0 \ \text{N/m}^3$$

has been applied only on the metal layer. From hydrostatics, the analytical solution of the vertical interface displacement (m) is

$$Dz(x) = -0.00637 \cdot x^2 + 0.03398 \,. \qquad (12)$$

The comparison of the model prediction to the bath-metal interface deformation with the analytical solution is shown in Figure 4. They are in good agreement.

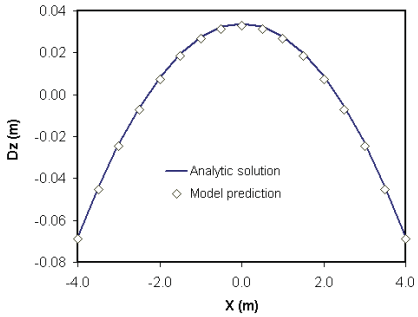

Figure 4: Comparison of the bath-metal interface deformation by analytic solution and model prediction.

Results for the revised benchmark case

Simplified anode configuration

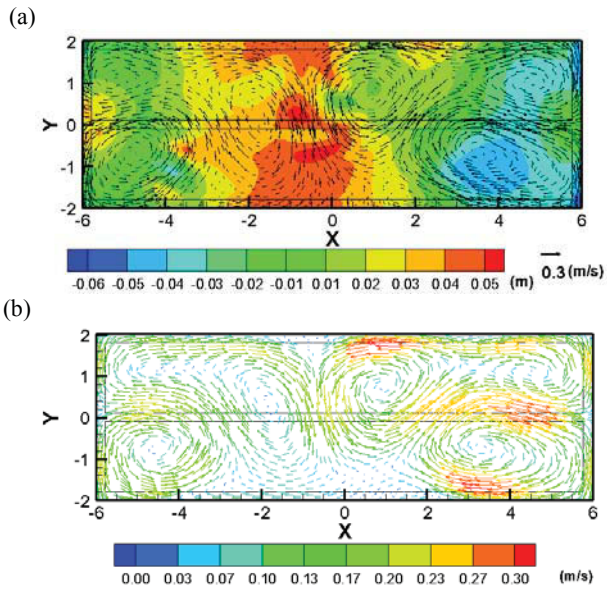

Figure 5: (a) Bath-metal interface deformation (contour plot) and liquid flow pattern (vectors) and
(b) Flow pattern in the vertical centre of the liquid metal predicted by the model for the revised benchmark case.

At first, the case with two large anodes (neglecting the cross-channels) is calculated. Here, as well as in all following applications, the distance between anode bottom and metal interface (ACD) was kept constant. This corresponds to the quasi-stationary condition in real cells after a sufficient time period after the last anode change.

The resulting dome shaped metal pad and velocity pattern on the interface is shown in Figure 5a, the flow at half height in the liquid metal in Figure 5b.

The metal heaving is close to 10 cm, the maximum velocity in the metal layer around 31 cm/s and the mean velocity about 14 cm/s. These are typical values expected for real cells. It can be speculated that the use of the k-ε turbulence model has a certain local impact on the interface shape as reported in [4].

Realistic anode configuration

The results for metal pad deformation and flow pattern is shown in Figure 6. The metal heaving is close to 11 cm. The maximum velocity in the metal layer is around 31cm/s and the mean velocity about 14 cm/s. When comparing to Figure 5, it is obvious that the cross-channels don't change the pattern qualitatively, nevertheless local details are modified. The maximum and mean velocity in the metal is unchanged

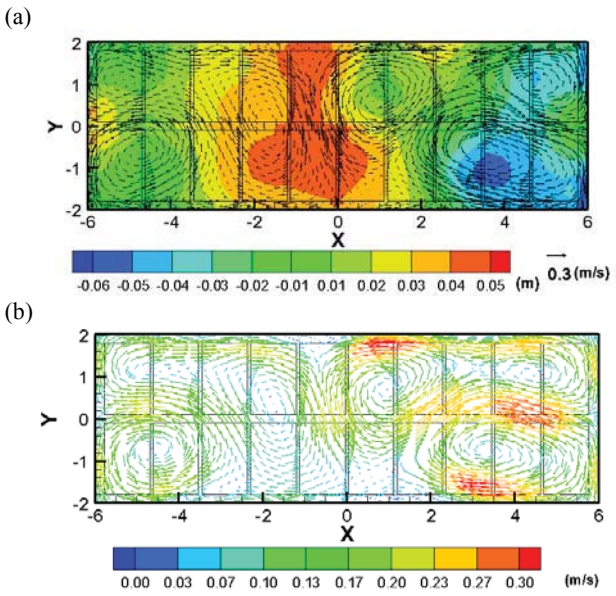

Figure 6: (a) Bath-metal interface deformation (m) and liquid flow pattern (vectors) and
(b) Liquid metal flow pattern, predicted by the model with detailed cross channels.

Lorentz force distribution

The metal pad deformation originates from the differences of the Lorentz forces between bath and metal. The horizontal Lorentz forces on the metal/bath interface and in the center of metal are presented in Figure 7. The well-known diverging character of the forces is visible.

(a)

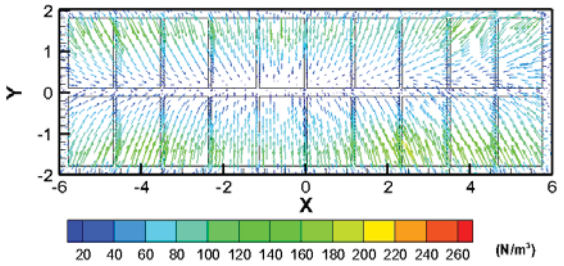

(b)

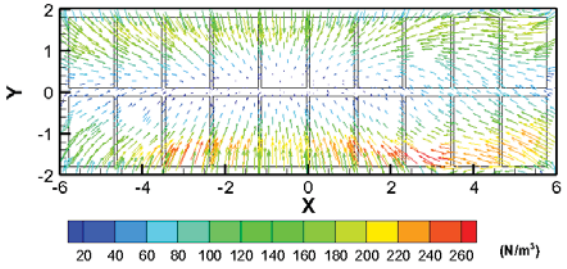

Figure 7: Distribution of Lorentz force horizontal components on
(a) the metal-bath interface and
(b) the middle plane of liquid metal layer.

Current density distributions

Figure 8 gives an impression of the electric current distribution in the metal layer and on various vertical cross-sections. In the areas of high velocities, a significant contribution of the induced currents is visible. A complete overview of the induced currents in the metal is given in Figure 9.

(a)

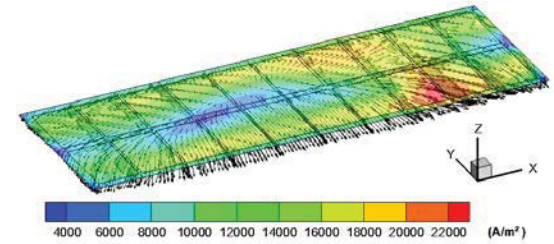

(b)

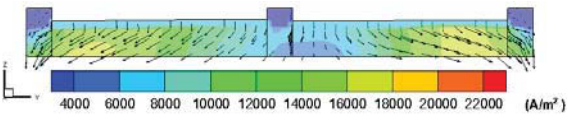

(c)

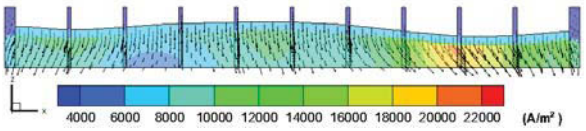

Figure 8: Distributions of current density on
(a) the horizontal plane in the middle of liquid metal
(b) the vertical plane at x=-0.5m and
(c) the vertical plane at y=-0.5m. The contour plot (c) is not displayed to scale.

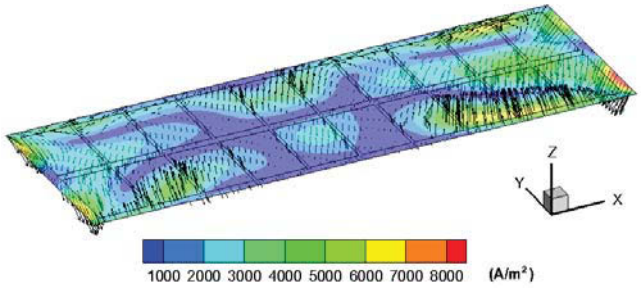

Figure 9: Distributions of induced current density on the middle horizontal plane (z=0.1m), in the liquid metal layer.

Conclusion

A revised benchmark problem for modeling of the stationary metal flow and metal pad heaving is given. The information of the underlying assumptions and boundary conditions should allow for recalculation with a suitable CFD-code. Due to the complexity of the metal heaving phenomena, it is not claimed that the given set-up will be sufficient for a quantitative calculation. The main advanced elements included here are constant ACD to avoid unphysical anode current redistribution in the model and induced currents. The inclusion of cross-channels between the anodes has only minor impact on the results.

Acknowledgement

The present work was supported by the project “Gas and Alumina distribution and transport” (GADT), financed by the Research Council of Norway, Institute for Energy Technology and Hydro Primary Metal Technology. Permission to publish the results is gratefully acknowledged.

References

[1] M. Segatz, D. Vogelsang, C. Droste, and P. Baekler., Modelling of transient magneto-hydrodynamic phenomena in Hall-Héroult cells, Light Metals 1993:361-368, 1993.
[2] O. Zikanov, A. Thess, P.A. Davidson and D.P. Ziegler, A new approach to numerical simulation of melt flows and interface instability in Hall-Héroult cells, Metallurgical and Materials Transactions 31B:1541-1550, 2000.
[3] M. Segatz, C. Droste and D. Vogelsang, Magneto-hydrodynamic effect of anode set pattern on cell performance, Light Metals 1997: 429-435, 1997.
[4] D.S. Severo, V. Gusberti, A.F. Schneider, E.C. Pinto and V. Potocnik, Comparison of various methods for modeling the metal-bath interface, Light Metals 2008: 413-418, 2008.
[5] S.B. Pope, Turbulent Flows, Cambridge University Press, 2000.
[6] V. Bojarevics and K. Pericleous, Solutions for the metal-bath interface in aluminium electrolysis cells, Light Metals 2009: 569-574, 2009.